Available online at www.sciencedirect.com
SCIENCE DIRECT®
International Journal of Solids and Structures 42 (2005) 5734–5757
INTERNATIONAL JOURNAL OF SOLIDS and STRUCTURES
www.elsevier.com/locate/ijsolstr

Effect of inertia and gravity on the draw resonance in high-speed film casting of Newtonian fluids

Fang Cao[a], Roger E. Khayat [a,*], J.E. Puskas [b]

[a] *Department of Mechanical and Materials Engineering, The University of Western Ontario, London, Ontario, Canada N6A 5B9*
[b] *Department of Chemical and Biochemical Engineering, The University of Western Ontario, London, Ontario, Canada N6A 5B9*

Received 16 June 2004; received in revised form 25 October 2004
Available online 17 May 2005

Abstract

The interplay between inertia and gravity is examined for Newtonian film casting in this study. Both linear and nonlinear stability analyses are carried out. Linear stability analysis indicates that while both inertia and gravity enhance the stability in film casting, inertia plays a more dominant role regarding the critical draw ratio. In contrast, the disturbance frequency is more sensitive to the effect of gravity. The nonlinear results show that at the critical draw ratio, the system oscillates harmonically, indicating the onset of a Hopf bifurcation. For a draw ratio above criticality, finite-amplitude disturbances are amplified, and sustained oscillation is achieved. It is found that the growth rate increases with draw ratio, but decreases with inertia and gravity, which suggests that initial transients tend to take longer to die out for a fluid with inertia and gravity. Transient post-critical calculations show that the nonlinearity can be effectively halted by inertia and gravity. The oscillation frequency (film-thickness amplitude) decreases (increases) with draw ratio. However, the film oscillates more frequently but less fiercely with stronger inertia and gravity effects. The rupture of the film is also examined, and is found to be delayed by inertia and gravity. Interestingly, although the oscillation amplitude is found to be weakest at the chill roll, it is at this location that the film tends to rupture first.

Keywords: Fiber spinning; Elongational flow; Nonlinear; Transient; Free surface

1. Introduction

One of the most important stages in the film-casting process is the film stretching through the air gap (between the extrusion die and the chill roll). Molten polymer extruded through a slit die is quenched

* Corresponding author. Tel.: +1 519 661 2111x88253; fax: +1 519 661 3020.
E-mail address: rkhayat@eng.uwo.ca (R.E. Khayat).

0020-7683/$ - see front matter © 2005 Published by Elsevier Ltd.
doi:10.1016/j.ijsolstr.2005.03.046

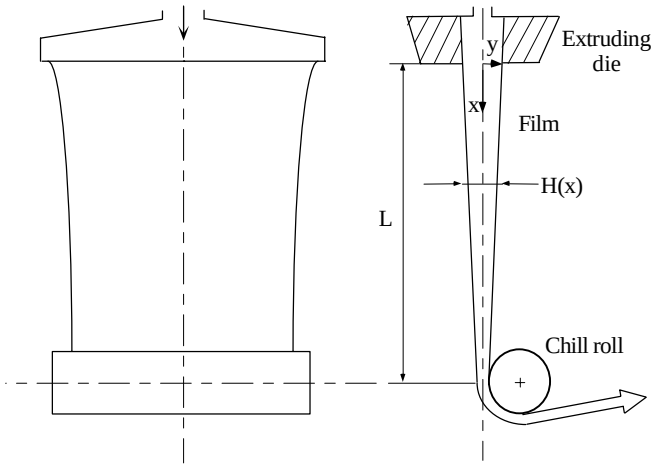

Fig. 1. Schematic illustration and coordinates used. Front and side views of the film-casting process.

and taken up by the chill roll, as illustrated in Fig. 1. Since the take-up velocity is much greater than the velocity at the die exit, the molten film is drawn uniaxially and conservation of mass requires a change in cross-sectional area. Thus, the film thickness is reduced to a desired value at the take-up point by choosing the appropriate draw ratio (ratio of the take-up velocity to the velocity at the die exit). The film casting operation is frequently limited at high take-up rates by an instability known as "draw resonance", which is characterized by an oscillatory variation in the film thickness. There exists a critical draw ratio, beyond which stable operation is impossible. When this draw ratio is exceeded, the "draw resonance" phenomenon occurs and spatio-temporal periodic variation in film thickness is observed.

Although numerous studies have been done on a similar process—fiber spinning, existing works related to film casting are limited. The first stability analysis of film casting was performed by Yeow (1974). Surface tension, aerodynamic drag, gravity and inertia were neglected in his study. Also, small film curvature and uniform axial stress across the film thickness were assumed. The analysis has confirmed the importance of the draw ratio D_R in controlling the onset of draw resonance. The theoretical results for casting a Newtonian fluid under isothermal, constant-force conditions show that the process is unstable for a draw ratio greater than a value of 20.21, which is identical to the critical value of fiber spinning.

However, it is well known that commercial film casting can be operated at a draw ratio larger than 20.21 without encountering instability. Several factors can contribute to this enhanced stability. Chief among these is the non-Newtonian behavior of the material being cast (Aird and Yeow, 1983). Extensive work has been done to investigate the non-Newtonian effects stemming from shear-thinning or viscoelastic effects. Another important factor is inertia effect, which has been neglected in the literature. Inertia becomes particularly important in modern high-speed film casting, and is the main object in the present study. Aird and Yeow (1983) examined the film casting of an inelastic power-law fluid. They derived an analytical steady-state solution and carried out a linear stability analysis. It was found that the critical draw ratio increases with the power-law index. The analysis also showed that for a power-law index greater than 1.2, disturbance waves were present across the film width. The influence of viscoelasticity on draw resonance was investigated by Anturkar and Co (1988), who conducted a linear stability analysis for isothermal film casting of a modified convected Maxwell fluid. They found that film casting is stable below a lower critical draw ratio and above an upper critical draw ratio. Their results also showed that shear thinning fluids are more unstable since shear thinning enlarges the region of instability, and they stated that fluids with higher characteristic time are more stable.

Later, Alaie and Papanastasiou (1991) studied the film casting of a BKZ-type fluid in an isothermal and non-isothermal steady-state analysis. It was concluded that thinning of the extruded film is enhanced by shear thinning and by air-cooling often down to solidification at about the glass transition temperature, upstream the chilling roll. The required tension decreases with shear thinning and increases with relaxation time. The temperature profile along the film departs from linear as the temperature of the cooling air decreases to about the ambient level.

Regarding Newtonian films, Barq et al. (1990) conducted a nonlinear stability analysis for isothermal Newtonian film casting. They used a finite-difference method to solve the time-dependent governing equations. The steady-state solution at a predicted draw ratio was used as the initial condition. The disturbance was introduced by changing the velocity at the take-up point (thus varied the draw ratio because the extrusion velocity was held constant in their study). For a step increase of 10% in the take-up velocity, the numerical results indicated that for final draw ratios below 20.3, the disturbances decayed with time and a new steady state was reached. For a final draw ratio of 20.3, the film thickness exhibited a sustained oscillation. For final draw ratios greater than 20.3, the amplitude of oscillation increased with time, and a sustained oscillation was attained after a long time. These results agreed with the stability limits obtained by the linear stability analysis of Yeow (1974) for isothermal Newtonian film casting.

Steady state and stability analyses of film casting of a modified Giesekus fluid were carried out by Iyengar and Co (1993, 1996). Both linear stability analysis for infinitesimal perturbations and nonlinear analysis for finite-amplitude disturbances were studied. In the linear analysis, the eigenvalue problem was treated as an initial-value problem (the standard approach used by the former researchers and scientists), and the numerical procedures involved a fourth-order Runge–Kutta algorithm with adaptive step-size control and Newton's iterations. The linear stability analysis indicates that extensional-thickening elongational viscosity enhances stability, whereas extensional-thinning elongational viscosity or shear-thinning shear viscosity reduces stability. A finite-element scheme was used in the nonlinear stability analysis to discretize the time-dependent partial differential equations. The disturbance was introduced by varying the draw ratio either as a step disturbance (the draw ratio was increased by 10% over a single time step) or as a ramp disturbance (the 10% increase in draw ratio was achieved by increasing the draw ratio linearly over 50 or more time steps). Similar nonlinear behaviors as those by Barq et al. (1990) were obtained for Newtonian film casting. For both Newtonian fluids and modified Giesekus fluids, the stability limits predicted by the linear stability analysis for infinitesimal disturbances were validated by the nonlinear stability analysis for finite-amplitude disturbances. Also, the growth rate and frequency of oscillation predicted by the linear analysis were found to agree with those predicted by the nonlinear analysis.

Inertia effect has been widely ignored in the literature. It can, however, have a significant role on the stability picture, and its value may still be small but not negligible. In the present study, the interplay between inertia and gravity is examined for Newtonian film casting. It will be shown that inertia has an important stabilizing influence on the film flow, even at small Reynolds number (e.g., for $Re = 0.25$ and $Fr = 0.10$, $D_R^C = 98.982$). The effect of inertia may explain the discrepancy between theory and experiment, especially in modern high-speed film casting. Both linear and nonlinear stability analyses are carried out. The current work is devoted to the interplay between inertia and gravity, and will therefore be restricted to Newtonian fluids.

2. Governing equations and boundary conditions

In this section, the general formulation is implemented for isothermal Newtonian fluid film casting as depicted in Fig. 1. The equations and boundary conditions are deduced taking into account inertia and gravity. In the film-casting process, the width of the film is very large compared with its thickness and is often much larger than the distance between the die and the chill roll (air gap). The film contraction

(neck-in) in the spanwise direction can thus be neglected, and the flow can be considered as two dimensional. Note in this case that the edge bead phenomenon will not be accounted for. Die swell can also be neglected given the small thickness of the film.

Consider the isothermal thin-film flow of an incompressible Newtonian fluid of density ρ and viscosity μ. In this study, inertia and gravity are assumed to be relatively important compared to surface tension effect. The film thickness and velocity are, respectively, H_0 and U_0 at the channel exit. The film length (air gap) between channel exit and take-up point is L. Here L and H_0 will be taken as the length scales in the streamwise, x, and depthwise, y, directions, respectively. The reference velocity and time will be taken as U_0 and L/U_0, respectively. In this case, the thin-film equations of relevance to the problem reduce to the following dimensionless form, namely, the continuity equation

$$u_x + v_y = 0, \tag{1}$$

and momentum conservation equation in the x direction

$$\frac{Re}{4} h\left(u_t + uu_x - \frac{1}{Fr}\right) = (hu_x)_x, \tag{2}$$

where u and v are the dimensionless velocities in the streamwise and depthwise directions, respectively, h is the dimensionless film thickness, t is the dimensionless time, and subscripts denote partial differentiation. Note that since elongational flow is the dominant mechanism (relative to shearing), u is taken to depend only on x and t. There are three similarity parameters in the problem, namely, the Reynolds number, Re, the Froude number, Fr, and the draw ratio, which are given by

$$Re = \frac{\rho U_0 L}{\mu}, \quad Fr = \frac{U_0^2}{gL}, \quad D_R = \frac{U_L}{U_0}, \tag{3}$$

where U_L is the velocity at the chill roll. The boundary conditions are prescribed as follows. At the die exit and the chill roll, the velocity is prescribed. The film thickness is given at the die exit only, so that

$$u(t, x = 0) = 1, \quad u(t, x = 1) = D_R, \quad h(t, x = 0) = 1. \tag{4}$$

Since $v = \mathrm{d}h/\mathrm{d}t$ at the free surface, the continuity equation and the kinematic condition can be combined to give (Middleman, 1977)

$$h_t + (hu)_x = 0. \tag{5}$$

Appropriate initial conditions will be imposed later.

3. Solution procedure

In this section, both steady state and linear stability analyses are discussed. The solution procedure for the nonlinear problem is then covered in some detail. Given the unavailability of the steady-state solution in analytical form in the presence of inertia and gravity, the steady state is obtained as part of the eigenvalue problem for linear stability analysis.

3.1. Linear stability analysis and the eigenvalue problem

The stability of the steady state is linearly analyzed. In this case, the film thickness and velocity are written as

$$h(x,t) = h^s(x) + \psi(x)\mathrm{e}^{\lambda t}, \quad u(x,t) = u^s(x) + \varphi(x)\mathrm{e}^{\lambda t}, \tag{6}$$

where h^s and u^s are the steady-state solutions, ψ and φ are complex perturbation amplitudes, and λ is the complex eigenvalue in the problem (λ_r being the growth or decay rate, and λ_i, the disturbance frequency). The equations governing the steady-state flow are determined from Eqs. (2) and (5), which reduce to

$$\frac{Re}{4}h^s\left(u^s\frac{du^s}{dx}-\frac{1}{Fr}\right)=h^s\frac{d^2u^s}{dx^2}+u^s\frac{dh^s}{dx},\quad h^s\frac{du^s}{dx}+u^s\frac{dh^s}{dx}=0. \tag{7}$$

The corresponding boundary conditions are readily obtained from (4), which are given by

$$u^s(x=0)=1,\quad u^s(x=1)=D_R,\quad h^s(x=0)=1. \tag{8}$$

In this case, the second equation in (7) is readily integrated to give a relation between the velocity and the thickness, namely $h^s(x)=1/u^s(x)$. Upon substitution of expressions (6) into Eqs. (2) and (5), the perturbation variables are found to satisfy the following linearized differential equations:

$$u^s\frac{d\psi}{dx}+\left(\lambda+\frac{du^s}{dx}\right)\psi+h^s\frac{d\varphi}{dx}+\frac{dh^s}{dx}\varphi=0, \tag{9}$$

$$h^s\frac{d^2\varphi}{dx^2}+\left(\frac{dh^s}{dx}-\frac{Re}{4}\right)\frac{d\varphi}{dx}-\frac{Re}{4}h^s\left(\lambda+\frac{du^s}{dx}\right)\varphi+\frac{du^s}{dx}\frac{d\psi}{dx}+\left[\frac{d^2u^s}{dx^2}-\frac{Re}{4}\left(u^s\frac{du^s}{dx}-\frac{1}{Fr}\right)\right]\psi=0, \tag{10}$$

with corresponding boundary conditions

$$\psi(x=0)=\varphi(x=0)=\varphi(x=1)=0. \tag{11}$$

The system of linear homogeneous equations (9) and (10), and the homogeneous boundary conditions (11) constitute an eigenvalue problem. A variety of solution methods can be applied to solve the eigenvalue problem, most of which treat it as an initial-value problem. See, for instance, references (Gelder, 1969; Shah and Pearson, 1972; Fisher and Denn, 1975) for fiber spinning, and references (Yeow, 1974; Aird and Yeow, 1983; Anturkar and Co, 1988; Iyengar and Co, 1993; Iyengar and Co, 1996) for film casting. Gelder (1969) solved the problem by using a finite-difference approximation, while Fisher and Denn (1975) applied a Runge–Kutta method, combined with a shooting technique. In this study, however, the problem is solved as a nonlinear two-point boundary-value problem.

Since only the critical conditions for the onset of instability are sought, then one sets $\lambda_r=0$ and $D_R=D_R^C$ in the analysis. The resulting augmented eigenvalue problem is cast in the following form (recall that $h^s=1/u^s$)

$$\frac{d\psi}{dx}=\frac{\gamma}{(u^s)^3}\varphi-\frac{\tau}{(u^s)^2}-\frac{(\lambda_i+\gamma)}{u^s}\psi, \tag{12}$$

$$\frac{d\varphi}{dx}=\tau, \tag{13}$$

$$\frac{d\tau}{dx}=\left[\frac{Re}{4}u^s+\frac{\gamma}{u^s}\right]\tau+\frac{Re}{4}(\lambda_i+\lambda)\varphi-\gamma\frac{d\psi}{dx}+\left[\frac{Re}{4}\left(u^s\gamma-\frac{1}{Fr}\right)-\frac{d\gamma}{dx}\right]\psi, \tag{14}$$

$$\frac{du^s}{dx}=\gamma, \tag{15}$$

$$\frac{d\gamma}{dx}=\frac{\gamma^2}{u^s}+\frac{Re}{4}\left(u^s\gamma-\frac{1}{Fr}\right), \tag{16}$$

$$\frac{dD_R^C}{dx}=0, \tag{17}$$

$$\frac{\mathrm{d}\lambda_{\mathrm{i}}}{\mathrm{d}x} = 0, \tag{18}$$

$$\psi(0) = \varphi(0) = \varphi(1) = 0, \quad u^{\mathrm{s}}(0) = 1, \quad u^{\mathrm{s}}(1) = D_{\mathrm{R}}^{\mathrm{C}}. \tag{19}$$

For given Re and Fr, there are seven real variable unknowns to be determined, including the critical draw ratio and frequency, and the steady-state velocity. Two boundary conditions are thus needed in addition to conditions (19). These are prescribed upon setting $\tau(0) = 1$ (without loss of generality since the equations are homogeneous), and noting that $D_{\mathrm{R}}^{\mathrm{C}}(0) = D_{\mathrm{R}}^{\mathrm{C}}(1)$. The resulting problem is of the two-point boundary-value type and is now nonlinear since both the frequency and draw ratio are part of the unknown variables. The problem is solved using a variable-order, variable-step size finite-difference scheme with deferred corrections. The basic discretization is the trapezoidal rule over a non-uniform mesh. The mesh is chosen adaptively, to make the local error approximately the same size everywhere. Higher-order discretization is obtained by deferred corrections. Global error estimates are produced to control the computation. The resulting nonlinear algebraic system is solved using Newton's method with step control. The linearized system of equations is resolved by a special form of Gauss elimination that preserves the sparseness.

3.2. Solution of the nonlinear problem

The nonlinear stability analysis consists of solving Eqs. (2) and (5) subject to conditions (4) and some initial conditions. An implicit forward-difference scheme in time is used to reduce the equations to the following third-order system:

$$\frac{\mathrm{d}u^k}{\mathrm{d}x} = \gamma^k, \tag{20}$$

$$\frac{\mathrm{d}\gamma^k}{\mathrm{d}x} = \frac{Re}{4}\left(\frac{u^k - u^{k-1}}{\Delta t} + u^k\gamma^k - \frac{1}{Fr}\right) + \frac{\gamma^k}{u^k h^k}\left(\frac{h^k - h^{k-1}}{\Delta t} + \gamma^k h^k\right), \tag{21}$$

$$\frac{\mathrm{d}h^k}{\mathrm{d}x} = -\frac{1}{u^k}\left(\frac{h^k - h^{k-1}}{\Delta t} + \gamma^k h^k\right). \tag{22}$$

The boundary conditions become

$$u^k(0) = h^k(0) = 1, \quad u^k(1) = D_{\mathrm{R}}. \tag{23}$$

Customarily, disturbances are introduced by varying the draw ratio, and the initial conditions for the time integration is the steady-state solution at the lower initial draw ratio. In the present study, instead, a finite-amplitude deviation from the steady-state solution at the prescribed draw ratio is added to the steady state to constitute the initial condition. For finite amplitude deviation, it means that the disturbances are comparable to the steady state. Eqs. (20)–(22), subject to conditions (23), constitute a two-point boundary-value problem, which is solved similarly to the eigenvalue problem as described earlier.

4. Discussion and results

In this section, results for steady flow and its linear stability are reported. The results for the flow in the post-critical range are also reported in terms of phase diagrams and time signature. The influence of the flow parameters on the oscillation amplitude and frequency is examined.

4.1. Steady-state flow

The influence of inertia on the steady film-casting flow is investigated by varying the Reynolds number over the range $Re \in [0, 2.0]$ while the draw ratio D_R is set equal to 20.0, and the gravity is neglected. The flow response is depicted in Fig. 2, where the distributions of the velocity, $u^s(x)$, and the film thickness, $h^s(x)$, are plotted against the position x. Since the viscosity of polymeric fluids varies from 10^2–10^6 P in the commercial fiber spinning and film casting processes (depending on the type of the polymer), the Reynolds number may have a wide range of values. For example, the Reynolds number of a Newtonian fiber spinning process in the experiment performed by Donnelly and Weinberger (1975) was reported to be less than 0.68×10^{-3}. However, in another paper, Doufas et al. (2000) carried out their simulation by using the data from the spinning of Nylon 66, and the Reynolds number in this case is estimated to be in the range

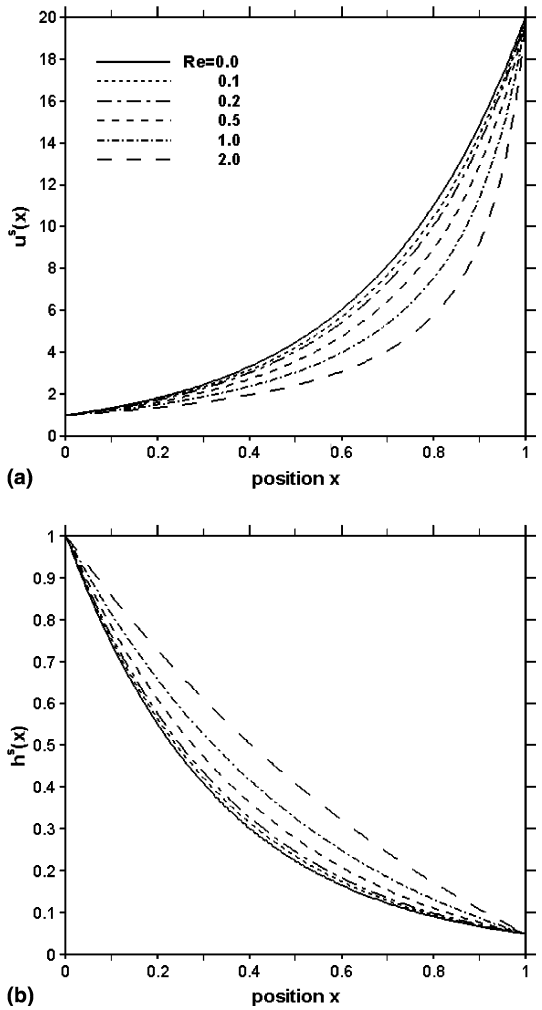

Fig. 2. Influence of inertia on the steady-state velocity, $u^s(x)$, and thickness, $h^s(x)$, distributions over the range $Re \in [0, 2.0]$ at $D_R = 20.0$ in the absence of gravity.

4.09–9.81. Hence, typical Reynolds number of practical interest are chosen for the present study, e.g. $Re = 0.1$, 0.2, 0.5, 1.0 and 2.0.

The results show that the velocity increases monotonically with the position x, at a rate that is relatively slower (faster) near the die exit (take-up point). At any fixed position x, the velocity decreases as Re increases. However, inertia clearly enhances stretching near the take-up point. Hence, films with higher inertia tend to break more easily. It is also observed that the velocity distribution deviates from the exponential behavior that is typical of creeping flow of single-layer films. Recall, in the absence of inertia and gravity, Eqs. (7) can be readily integrated, and the velocity and thickness are given by

$$u^s(x) = e^{x \ln D_R}, \quad h^s(x) = e^{-x \ln D_R}. \tag{24}$$

When inertia is included, one has

$$u^s(x) = \frac{C_1}{C_2 e^{-C_1 x} - \frac{Re}{4}}, \quad h^s(x) = \frac{C_2 e^{-C_1 x} - \frac{Re}{4}}{C_1}, \tag{25}$$

where C_1 and C_2 are integration constants, which can only be fixed numerically from the boundary conditions. However, approximate expressions can be obtained for a flow with dominant inertia (see below). Clearly, expressions (25) indicate that exponential behavior is recovered in the limit of vanishingly small inertia. The thickness profiles (Fig. 2(b)) show that under steady-state condition, the film thickness decreases with x, at any Reynolds number, at a rate that increases as the Reynolds number increases. More generally, in the presence of inertia, the overall velocity and thickness deviate from exponential behavior as Re increases, reflecting an intensification of the non-linear character of the flow. In fact, for large Re, expressions (25) reduce approximately to

$$u^s(x) = \frac{1}{1 + \left(\frac{1}{D_R} - 1\right) e^{\frac{Re}{4}(x-1)}}, \quad h^s(x) = 1 + \left(\frac{1}{D_R} - 1\right) e^{\frac{Re}{4}(x-1)}, \tag{26}$$

which indicate that the velocity increases with x very slowly essentially throughout the film length, but experiences a sudden jump near the take-up point. In contrast, the thickness decreases almost linearly at some Reynolds number. For larger Re, the thickness remains close to that at the exit throughout the film, and drops suddenly near the take-up point. Thus, a low-viscosity fluid tends to experience plug-flow conditions for most of the air gap, and exhibits strong necking near the take-up point. These observations confirm the vulnerability of the film near the chill roll for a flow with dominant inertia.

The effect of gravity is examined by varying the ratio Re/Fr while fixing the draw ratio $D_R = 20.0$, and neglecting inertia. Fig. 3 displays the velocity and film thickness distributions over the range $Re/Fr \in [0, 100]$. The steady-state velocity increases with the position x at any Re/Fr. The velocity increases due to gravity, deviating gradually from the exponential growth, to approach linear growth with x (for $Re/Fr > 100$). Simultaneously, the film thickness begins to decrease rather sharply near the die exit as gravity increases. It is found that the flow and thickness are not sensitive to the effect of gravity for $Re/Fr < 5$. In general, the effect of gravity is significant only when the ratio Re/Fr is large enough. Finally, it is important to note that the effect of gravity is opposite to that of inertia. While gravity tends to cause the film to neck in near the channel exit, inertia tends to cause the film to contract sharply near the take-up point.

4.2. Linear stability results

In this section, the influence of inertia and gravity on both the critical draw ratio and the corresponding disturbance frequency is discussed. The eigenvalue problem is treated as a two-point boundary-value problem. This approach is convenient, and its validity is established here upon comparison with results, in the absence of inertia and gravity, which are based on the initial-value method used in the literature. When

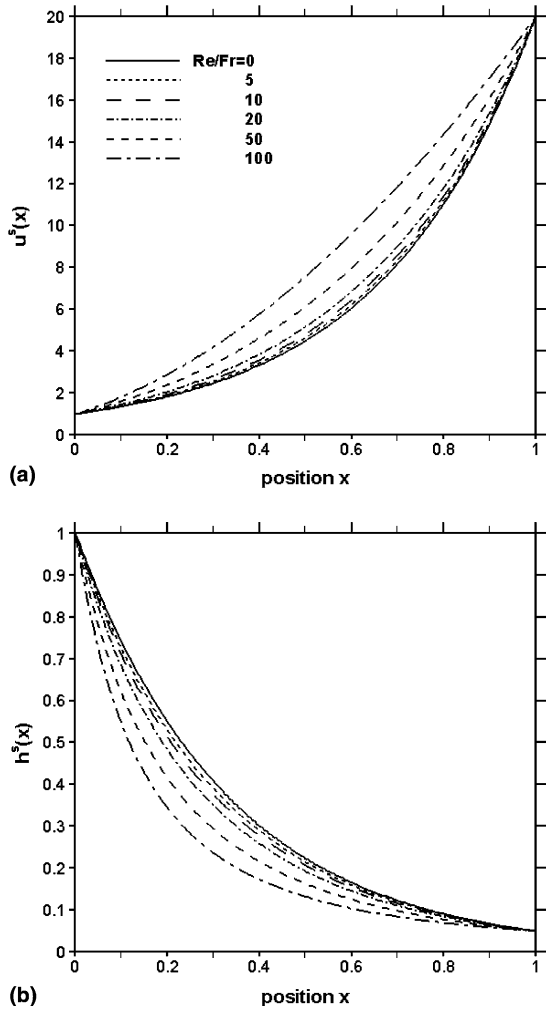

Fig. 3. Influence of gravity on the steady-state velocity, $u^s(x)$, and thickness, $h^s(x)$, distributions over the range $Re/Fr \in [0, 100]$ at $D_R = 20.0$ in the absence of inertia.

inertia and gravity are neglected, the critical draw ratio for film casting is identical to that of fiber spinning (Yeow, 1974). Comparison between the current results and those of Pearson and Matovich (1969) is given in Table 1 for the critical draw ratio, corresponding to different modes. These results are also compared

Table 1
Comparison of D_R^C at $Re = 0$ and $Fr \to \infty$ based on current formulation and the results of Pearson and Matovich (PM) (Pearson and Matovich, 1969), Fisher and Denn (FD) (Fisher and Denn, 1975) and Gelder (1969)

Mode	Current	PM	FD	Gelder
First	20.218	20.205	20.218	20.206
Second	50.120	49.985		50.000
Third	80.401	80.335		
Fourth	110.714	110.881		

with those of Fisher and Denn (1975) and Gelder (1969), which are obtained by treating the eigenvalue problem as an initial-value problem. There is good agreement between the two methods.

Consider now the influence of inertia and gravity on the critical draw ratio D_R^C. At the critical draw ratio, the real part of the eigenvalue passes from negative to positive. Below this value, all infinitesimal perturbations decay exponentially in time, while above this value, the first mode of the eigenfunction will be amplified exponentially with time. The second and higher eigenvalues are all negative at this draw ratio. When viscous effects are dominant, linear stability analysis predicts that $D_R^C = 20.218$.

The effects of inertia and gravity cannot always be neglected with respect to the viscous forces, especially when the spinning or casting air gap is large, and when the process is vertical. Although the weight of the fiber or film is generally small, the gravitational force can be important. During the spinning of a Newtonian sugar syrup, gravity can constitute as much as 75% of the total spinline force (Kumar and Gupta, 2003). Also, when the air gap is large (usually greater than 1 m in air drawing fiber spinning process), and the process is operated at high spinning or casting speeds, inertia effect is not negligible (Agassant et al., 1991).

The interplay between inertia and gravity on the stability of film casting is assessed by examining the dependence of the critical draw ratio D_R^C on both Re and Re/Fr. The neutral stability curves, which separate the stable and unstable domains, are obtained over the ranges $Re \in [0, 0.25]$ and $Re/Fr \in [0, 25]$. These ranges correspond to most situations of practical interest (Shah and Pearson, 1972; Doufas et al., 2000). Inertia and gravity effects show that there is a significant stabilization of the process. This is illustrated in Fig. 4, where the critical draw ratio is plotted against Re and Re/Fr (3D plot in Fig. 4(a)), and against Re, for different levels of gravitational effect (Fig. 4(b)). It is predicted that at any Re/Fr, D_R^C increases with Re, which indicates that draw resonance is delayed by inertia. The dependence of the critical draw ratio on Re is more sensitive when gravitational effect is stronger. Moreover, at a fixed Re, D_R^C increases as Re/Fr increases, which suggests that gravity also helps stabilize the process. The process is expected to become unstable if the film is operated at a draw ratio that exceeds the predicted D_R^C level. The fact that inertia and gravity have a stabilizing influence, may then explain the discrepancy between the linear stability analysis results for creeping flow and the practical process. In practice, it is found that the critical draw ratio is higher than 20.21 (Aird and Yeow, 1983; Shah and Pearson, 1972). Fig. 4 also shows that even small inertia and gravity effects can be strongly stabilizing. For instance, the critical draw ratio reaches 56.27 for film casting at only $Re = 0.20$ and $Re/Fr = 20$. Note that the value of Re/Fr could reach in reality a level as high as 30 and even larger according to Shah and Pearson (1972). A notable observation from Fig. 4 is that gravity remains mildly stabilizing until the ratio Re/Fr becomes large enough. The growth of D_R^C with Re is basically exponential, and it decreases with Fr roughly like $\exp(-13.6Fr)$.

In the absence of gravity ($Fr \to \infty$), the critical draw ratio reaches a high value for small inertia flow, such as 316.9 at $Re = 0.4$. Since the typical draw ratio in an industrial film casting process is about 28.0–31.0 for polypropylene and somewhat higher for polyethylene, theoretically, it can be concluded that for $Re > 0.40$, the film-casting process is stable for all practical purposes. These values clearly illustrate the stabilizing role of inertia. Gravity is found to remain mildly stabilizing until the value of Re/Fr becomes large enough ($Re/Fr > 5$ in the absence of inertia). Since the values of Re/Fr can have a wide range in polymer processes (spinning of Nylon 66 may have a very high value of Re/Fr (estimated between 89.0 and 213.0) (Doufas et al., 2000)), this shows that gravity also has a stabilizing effect. The results shown in Fig. 4 suggest that for industrial operations, although both inertia and gravity are stabilizing, inertia tends to be the more effective stabilizing force.

The dependence of disturbance frequency on inertia and gravity is shown in Fig. 5. The instability predicted takes the form of a traveling wave (overstability), coinciding with the onset of a Hopf bifurcation. The imaginary part of the eigenvalue, λ_i, gives the oscillating frequency of the disturbance. It is found that both inertia and gravity have obvious influences on the disturbance frequency. In Fig. 5, the disturbance frequency increases with Re at any Re/Fr value. Thus, the flow oscillates at a higher frequency with increasing

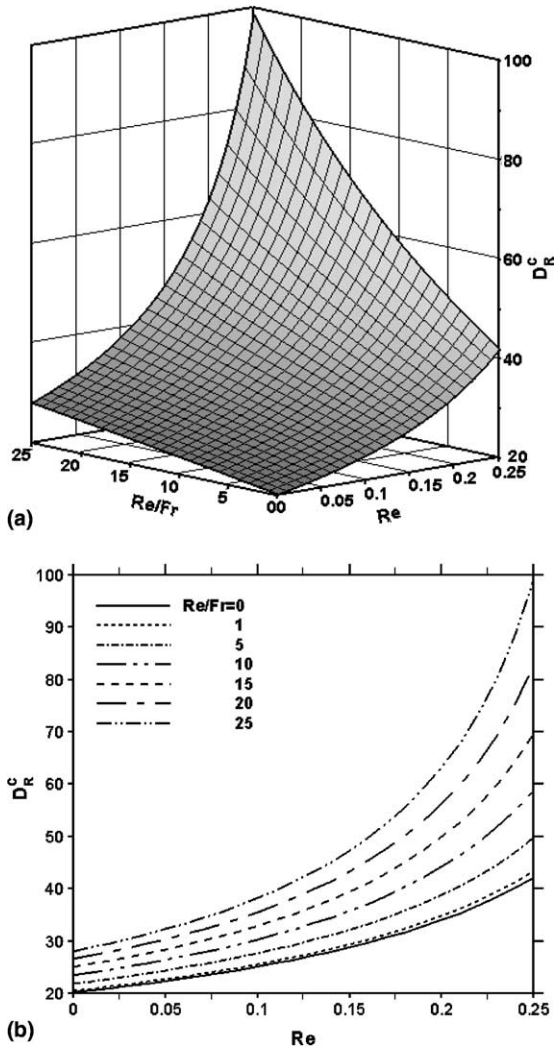

Fig. 4. Effect of inertia and gravity on critical draw ratio D_R^C over the range $Re \in [0, 0.25]$ for different gravitational levels, $Re/Fr \in [0, 25]$. A three-dimensional perspective is also shown.

inertia. Moreover, at a fixed Re, the disturbance frequency increases as Re/Fr increases, which indicates that the frequency also increases with gravity. In contrast to the case of the critical draw ratio, Fig. 5 shows that it is gravity, rather than inertia, that has a dominant effect on the disturbance frequency.

4.3. Nonlinear stability results

Linear stability analysis is useful only in predicting the onset conditions of the instability in film casting, but fails to predict the actual spatio-temporal response once criticality is reached (draw resonance). Given the linearity of the eigenvalue problem, the unstable disturbance simply grows exponentially without bound. A nonlinear stability analysis is conducted here to examine the stability of the system to finite-amplitude disturbances.

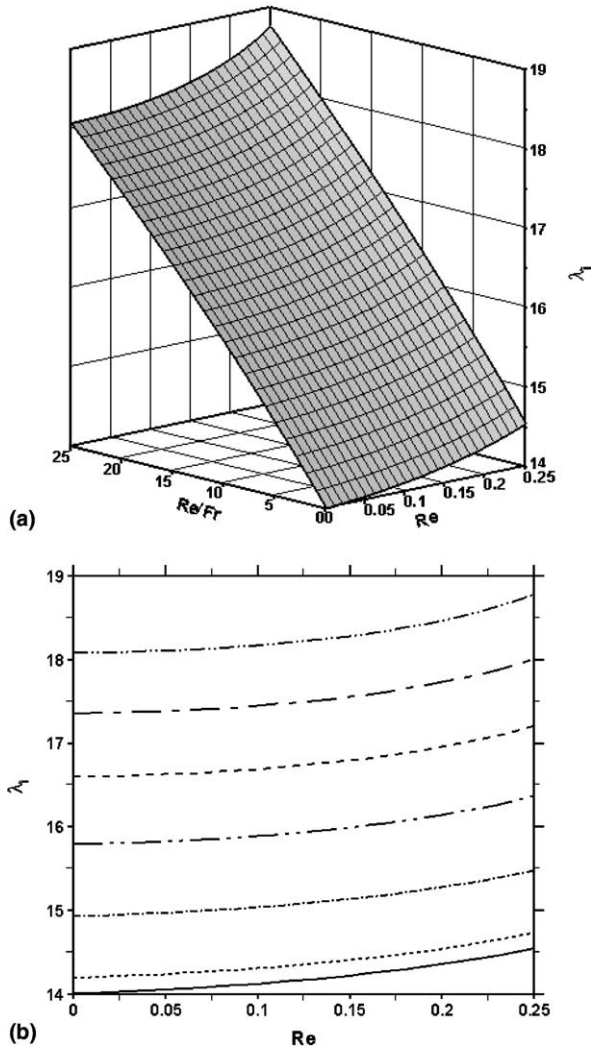

Fig. 5. Effect of inertia and gravity on disturbance frequency λ_i over the range $Re \in [0, 0.25]$ for different gravitational levels, $Re/Fr \in [0, 25]$. A three-dimensional perspective is also shown.

The disturbance is usually introduced by increasing the draw ratio. This means that the extrusion rate is held constant while the velocity at the take-up roll or chill roll is varied. Iyengar and Co (1996) examined the nonlinear response in the absence of inertia and gravity, using a finite-element approach to discretize the full equations spatially and integrating the resulting equations in time. The velocity and stress components were approximated with either linear or quadratic interpolating functions. This method, however, requires an excessively long time (1–10 h of CPU time) per run because of the small time step ($\Delta t = 0.01$) needed for convergence. In the present analysis, the system of nonlinear time-dependent partial differential equations is discretized using a finite-difference method and solved as a boundary-value problem. The disturbances are introduced by adding finite-amplitude disturbances onto the steady-state solutions. To obtain an accurate numerical result, an extremely small time step is used, i.e., $\Delta t = 0.0001$, which is one-hundredth of what Iyengar and Co (1996) used. The current solution is typically obtained in less than 1 h.

4.3.1. Transient response in the absence of inertia and gravity

The predictions of transient behavior in the case of negligible inertia and gravity are examined first. The nonlinear analysis is conducted for three draw ratios: 15.0, 22.0 and 30.0, corresponding to draw ratios below, near, and above the critical value. The response of the film thickness at the take-up point ($x = 1$) is displayed in Fig. 6. Linear stability analysis predicts the onset of a Hopf bifurcation (overstability) at the critical draw ratio. The figure shows that, for a draw ratio of 15.0, the film thickness at the take-up point exhibits damped oscillation. The disturbance decays with time, but remains symmetric with respect to the steady state, and after some 12 time units, the steady state is attained. For a draw ratio of 22.0, the disturbance is amplified and grows relatively slowly. Due to the slow growth of the amplitude, sustained oscillation will not be reached until a time large enough (about $t = 35$). Finally, for a draw ratio of 30.0, the amplitude of oscillation grows rapidly initially, and after some time the growth rate diminishes. Sustained oscillation is then achieved at about 10 time units. The nonlinear results are consistent with linear stability analysis. It is noted that beyond the critical draw ratio (in this case, $D_R = 30.0$), the sustained disturbance

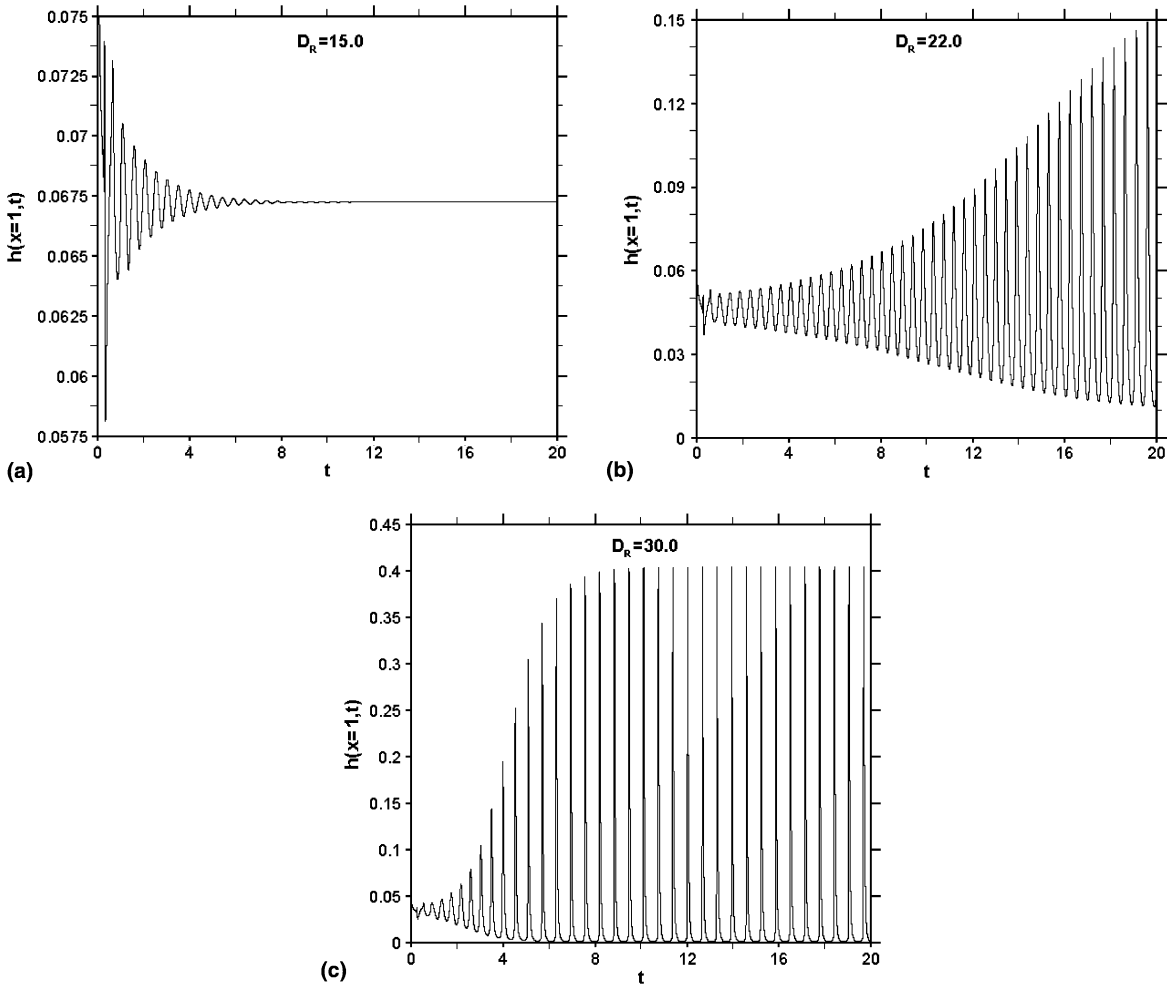

Fig. 6. Transient response of film thickness at take-up point $h(x = 1, t)$ for draw ratio (a) below, (b) slightly above, and (c) further beyond $D_R^C = 20.218$, in the absence of inertia and gravity.

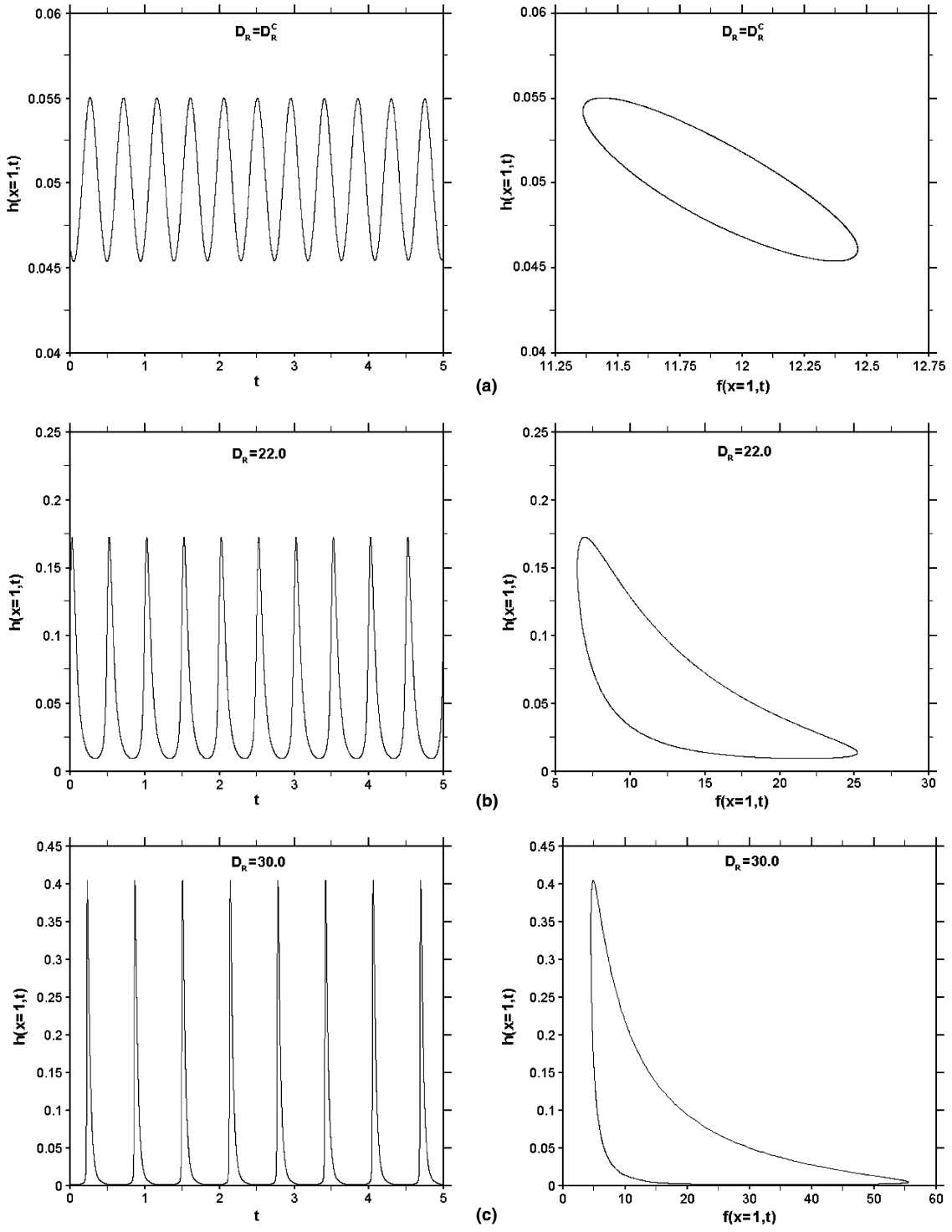

Fig. 7. Time signature of sustained oscillation and corresponding phase plots showing limit cycles at $D_R = D_R^C$ (a), 22.0 (b) and 30.0 (c) in the absence of inertia and gravity.

consists of narrow, sharp peaks alternating with wide, flat bottoms, reflecting a dissymmetry with respect to the steady state. Similar pulse-train response was predicted by Ishihara and Kase for Newtonian fiber spinning (Ishihara and Kase, 1975; Ishihara and Kase, 1976), and by Iyengar and Co for Newtonian film casting (Iyengar and Co, 1996).

The enlarged waveforms and the corresponding phase plots are shown in Fig. 7, where sustained oscillation is depicted at the critical draw ratio, 20.218, and $D_R = 22.0$ and 30.0. Both time signatures and phase portraits are included. In the phase plots, the film thickness is plotted against the axial tensile stress, $f(x,t)$, at the take-up point. The stress scale is chosen as $\mu U_L/L$. At criticality the oscillation is purely harmonic (elliptic limit cycle) and symmetric about the steady state. At the draw ratio just beyond criticality ($D_R = 22.0$), the wave peaks become sharper while the bottoms are flatter. The amplitude of the sustained oscillation increases with D_R and the oscillation is not symmetric any more. Deviation from the elliptical shape of the limit cycle reflects growing nonlinearities. It is observed that the film thickness tends to be large (small) when the tensile stress is small (large). When the draw ratio is further increased ($D_R = 30.0$), the

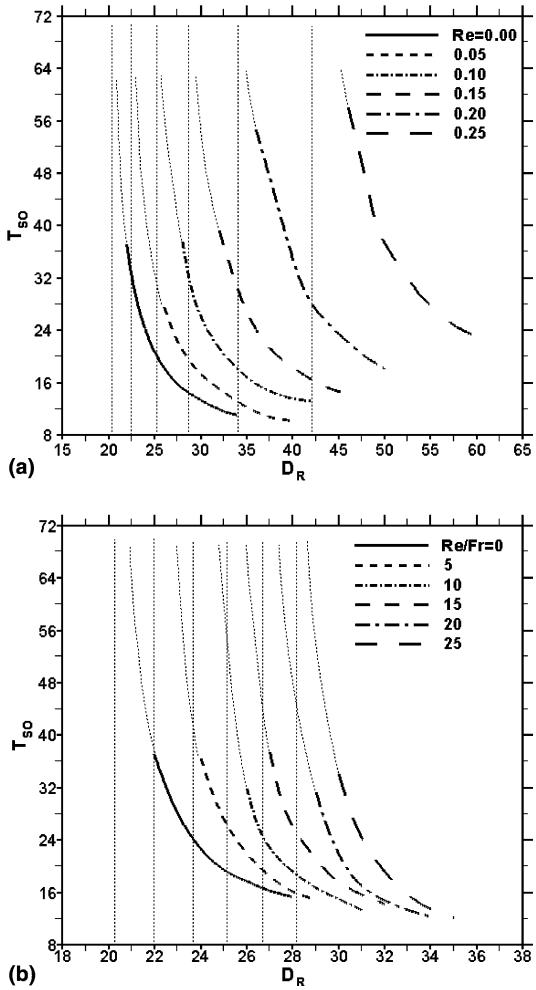

Fig. 8. Dependence of the time needed to reach sustained oscillation, T_{so}, on (a) D_R and inertia over the range $Re \in [0, 0.25]$, and (b) D_R and gravity over the range $Re/Fr \in [0, 25]$.

wave peaks become very narrow and sharp, with the wave bottoms becoming flatter. More importantly, the film thickness reaches practically a zero value for essentially most of the period of oscillation. This means that the film is predicted to rupture at $D_R = 30.0$.

4.3.2. Influence of inertia and gravity

It is observed that the rate of growth or decay toward sustained oscillation depends on the level of D_R beyond criticality, as well as on inertia and gravity effects. The same observation can be made for the pre-critical range. For $D_R > D_R^C$, the greater D_R is, the sooner the sustained oscillation is achieved. This can be clearly seen from Fig. 8, where the time needed to reach the sustained oscillation, T_{so}, decreases as D_R increases above D_R^C. Sustained oscillation is assumed to be reached when the relative difference between two successive peak values is less than 0.01%. The influence of inertia and gravity on T_{so} is shown in Fig. 8(a) and (b), respectively. At $D_R = D_R^C$, since the disturbances neither decay nor grow, the sustained oscillation is never reached, i.e., $T_{so} \to \infty$ when $D_R \to D_R^C$. The figure includes the dashed vertical lines corresponding to critical values. Fig. 8(a) shows that at any *Re* level (gravity neglected), T_{so} drops dramatically

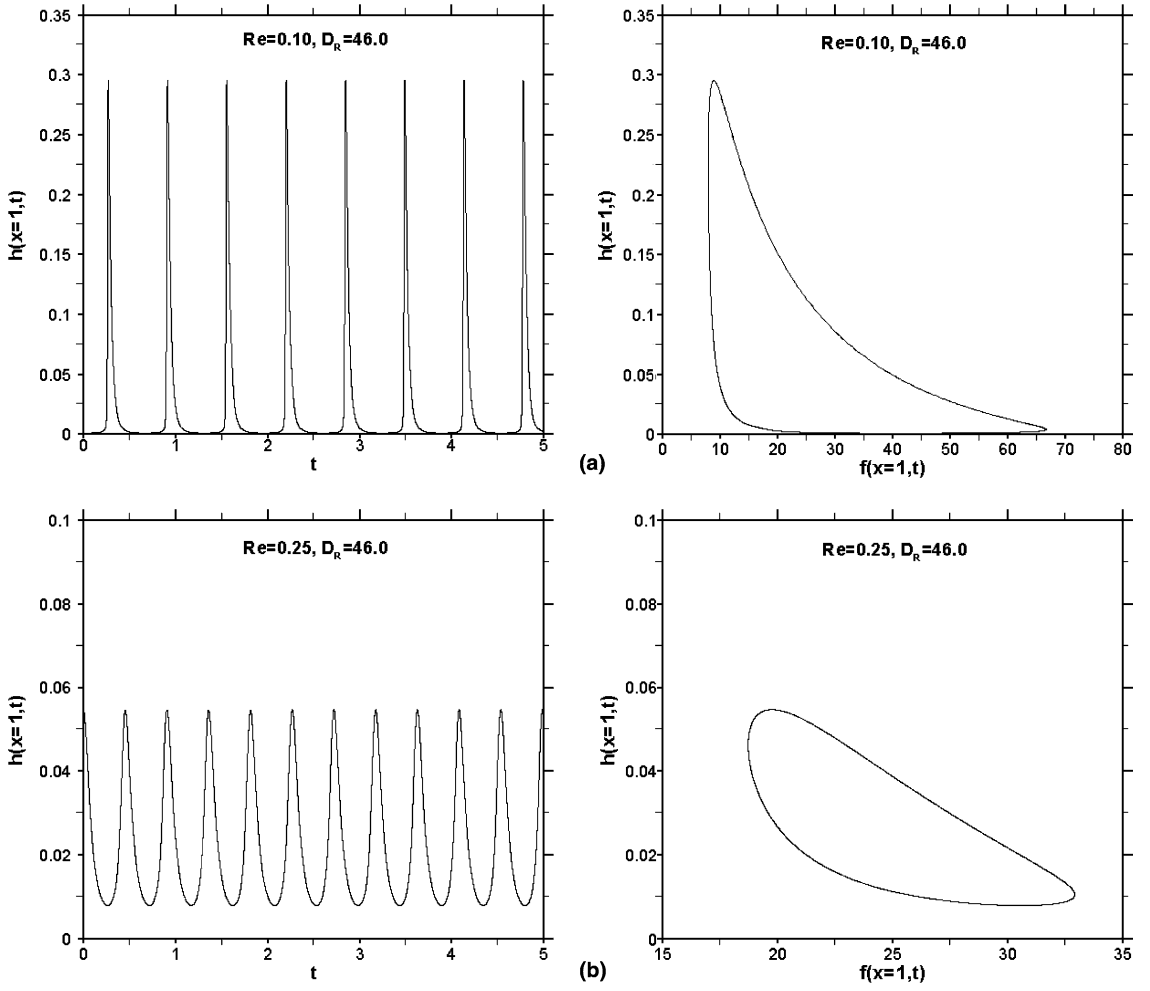

Fig. 9. Influence of inertia on sustained oscillation for $D_R = 46.0$ at (a) $Re = 0.10$, and (b) $Re = 0.25$, in the absence of gravity.

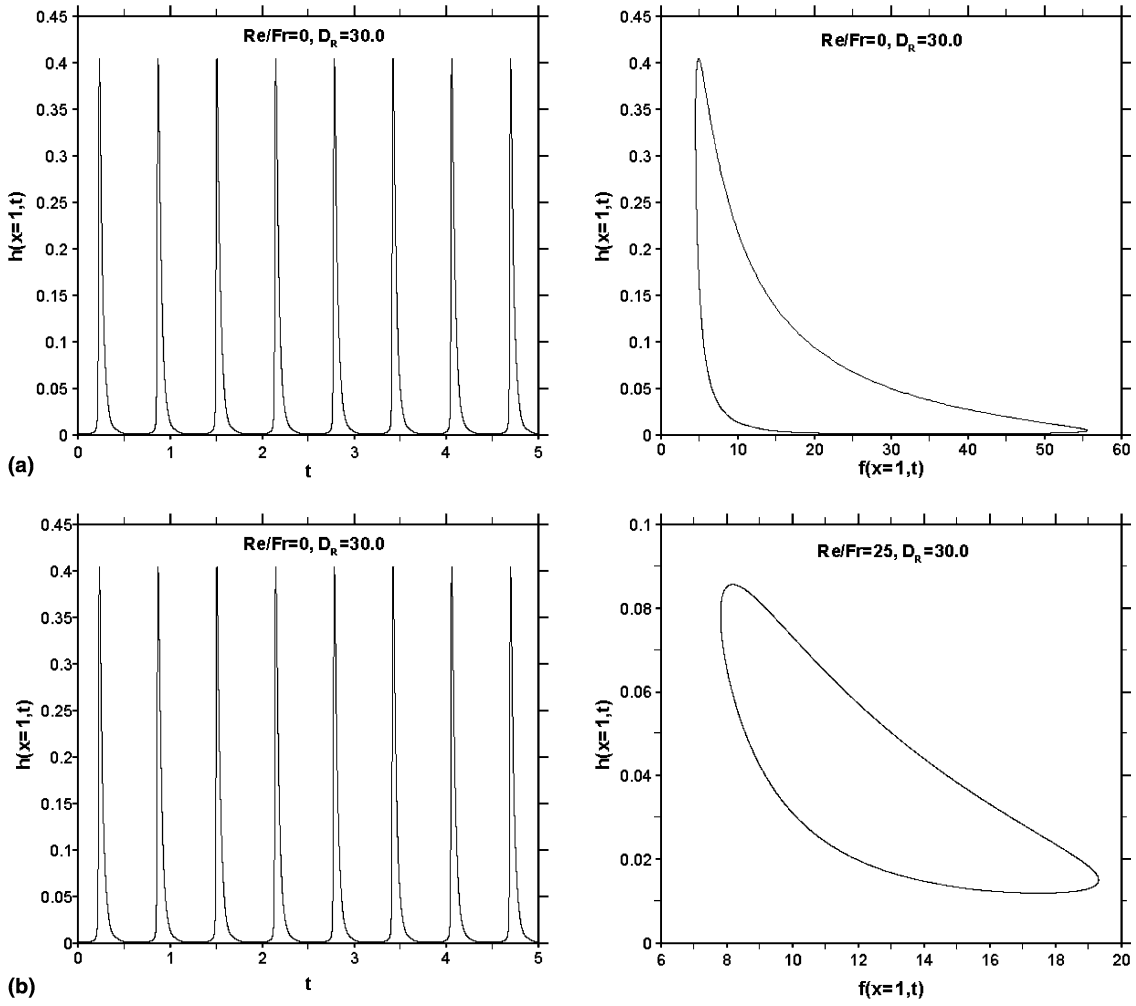

Fig. 10. Influence of gravity on sustained oscillation for $D_R = 30.0$ at (a) $Re/Fr = 0$, and (b) $Re/Fr = 25$, in the absence of inertia.

Table 2
Periods and frequencies predicted by linear and nonlinear analysis

Re (*Re*/*Fr*)		Critical D_R	Linear analysis		Nonlinear analysis	
Re	*Re*/*Fr*	D_R^C	Period (*T*)	Frequency (*f*)	Period (*T*)	Frequency (*f*)
0	0	20.218	0.448	14.011	0.449	14.005
0.1	0	25.076	0.445	14.127	0.446	14.104
0.2	0	33.938	0.438	14.359	0.439	14.298
0.1	10	30.343	0.395	15.895	0.399	15.761
0.2	10	56.267	0.354	17.731	0.355	17.680

near the critical value, and then decreases relatively mildly as D_R increases. This suggests that the draw resonance phenomenon cannot be clearly observed at a draw ratio close to the critical value until a very long time. The time needed to reach the sustained oscillation is shortened gradually as D_R further increases. Far

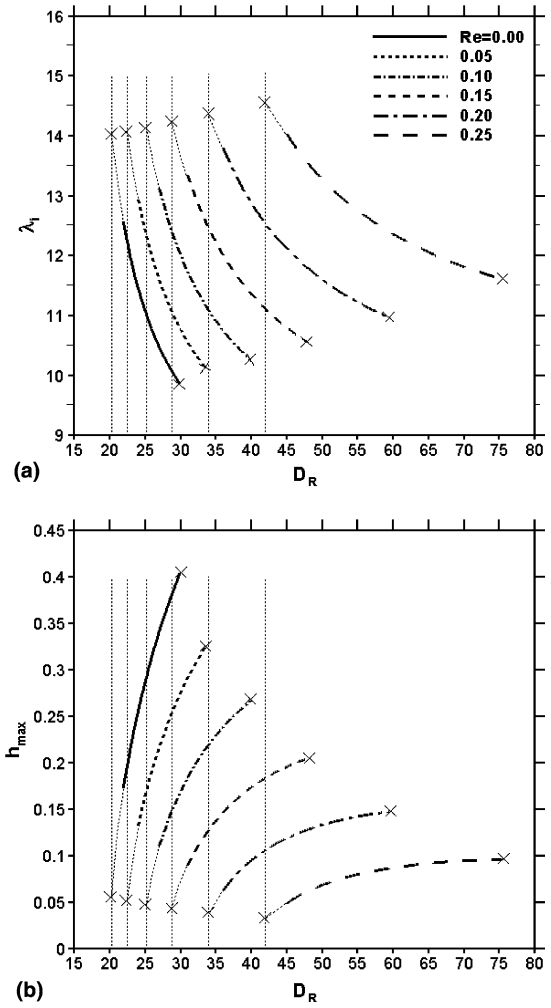

Fig. 11. Influence of draw ratio and inertia on (a) draw resonance frequency λ_i, and (b) film-thickness amplitude h_{max}, over the range $Re \in [0, 0.25]$ in the absence of gravity.

beyond criticality, the draw resonance occurs almost immediately. Meanwhile, for a fixed D_R, T_{so} increases with Re, which indicates that it takes longer to reach sustained oscillation as inertia increases; recall from linear stability analysis that inertia delays the onset of draw resonance. In Fig. 8(b), T_{so} is shown to decrease with D_R at any Re/Fr level, and increases with Re/Fr for a fixed D_R.

Further insight on the effect of inertia and gravity on the transient behavior of film casting is gained by examining the nonlinear flow. Consider the influence of inertia in the absence of gravity. The draw ratio is fixed at $D_R = 46.0$. The transient response is examined for $Re = 0.10$ and 0.25, with corresponding critical draw ratio 25.08 and 41.94, respectively. The results are shown in Fig. 9. For $Re = 0.10$, the flow is far above D_R^C, and the response is highly nonlinear. At $Re = 0.25$, the flow is closer to the critical threshold. In this case, the response is less nonlinear, with smaller oscillation amplitude and more restricted range in axial stress value. Similar observations can be made regarding the effect of gravity, as shown in Fig. 10.

The validity of the nonlinear solution methodology can be assessed upon comparing the values of the critical draw ratio and corresponding frequency based on the nonlinear solution against linear stability

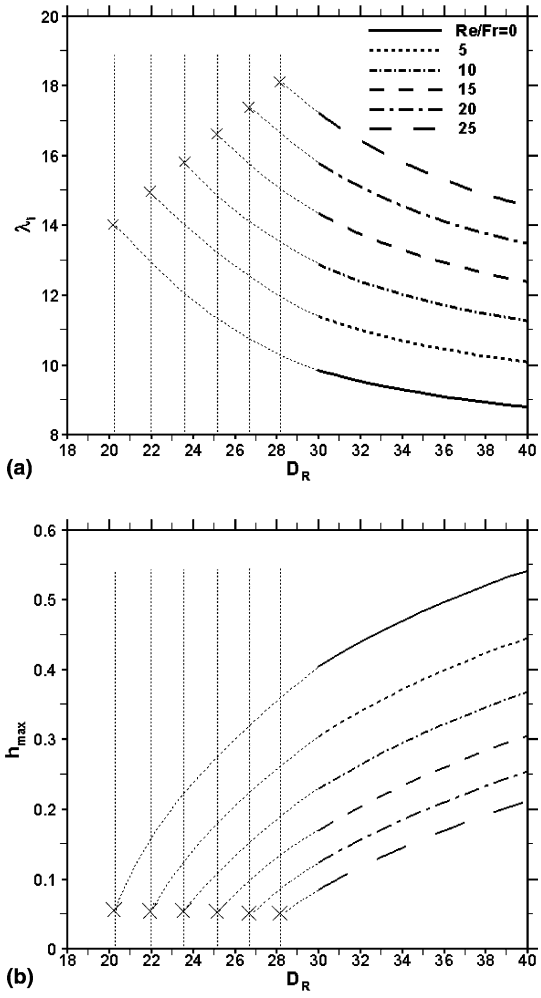

Fig. 12. Influence of draw ratio and gravity on (a) draw resonance frequency λ_i, and (b) film-thickness amplitude h_{max}, over the range $Re/Fr \in [0, 25]$ in the absence of inertia.

analysis. It is expected, however, that the detection of the onset of instability, and therefore the identification of the critical draw ratio, to be much more difficult than the determination of the oscillation frequency. The comparison between the linear and nonlinear results is summarized in Table 2, reflecting excellent agreement in the frequency values (to the second decimal).

The influence of inertia on the draw resonance frequency and the film-thickness amplitude is shown in Fig. 11, where the frequency λ_i and maximum film thickness h_{max} are plotted against D_R at different Re levels with $Fr \to \infty$ (gravity neglected). The curves have been extrapolated to the critical level, where they intersect with the vertical lines at $D_R = D_R^C$ for a given Re value. The figure shows that the oscillation frequency (thickness amplitude) decreases (increases) with the operating draw ratio. That is, for large D_R, the film loses its stability and oscillates relatively slowly but more violently, which suggests that the greater the draw ratio above D_R^C, the more drastic the draw resonance phenomenon becomes, leading eventually to film breakup. On the other hand, at a fixed D_R, the frequency (thickness amplitude) increases (decreases) with Re, which indicates that, if the film is stretched at the same draw ratio, a flow with higher inertia oscillates

at higher frequency with smaller film thickness variation. The frequency distributions are in agreement with predictions from linear stability analysis (see Fig. 5). It is interesting to observe from the figure that while the rate of decrease of the frequency with D_R is essentially independent of the level of inertia, the rate of increase of film amplitude is much slower for large Re. Similar observations can be made regarding the influence of gravity, as illustrated in Fig. 12, except unlike inertia, gravity, in this case, does not seem to affect the rate of dependence of the frequency and film amplitude on D_R.

It is observed from Figs. 11 and 12 that the ranges of draw ratio covered are different in each figure. On the one hand, the lower bound of the D_R range corresponds to the critical threshold, which depends strongly on inertia and gravity. On the other hand, the range does possess an upper bound beyond which the solution cannot be pursued. This corresponds to the practical process operation with a draw ratio that is far above criticality, resulting in film breakup. Since the film tends to be thinnest at the take-up point, then the breakup is most likely to occur at that point. In this work, the film is assumed to break up when the minimum film thickness reaches less than one-thousandth of that at the channel exit ($h < 0.001$). The draw ratio at which the film ruptures, $D_R = D_R^{Rup}$, can then be determined. Fig. 13 shows the relationship between D_R^{Rup} and Re for different Re/Fr levels. It is observed that inertia and gravity not only enhance film stability, but they tend to delay film rupture as well (see also Fig. 4). Similarly to the critical draw ratio D_R^C in Fig. 4, D_R^{Rup} is predicted to increase with Re. The increase appears to be exponential. When inertia is negligible, D_R^{Rup} increases with gravity rather linearly.

So far, the focus has been on the temporal response of the flow at a given position (take-up point) once the film becomes unstable. Further insight is gained by examining the actual shape of the film at different times, particularly in relation to the steady-state profile. It is first recalled that the steady film thickness decreases monotonically with position, from unity at the channel exit to $1/D_R$ at the take-up point. For oscillatory flow ($D_R > D_R^C$), the film profile over the entire air gap changes over the period T of sustained oscillation. This is illustrated in Fig. 14, where the film thickness is plotted against the position x at $t = 0$, $T/4$, $T/2$ and $3T/4$, for various flow conditions. The steady state is included for reference. Clearly, the film thickness appears to decrease monotonically with x under any condition and any time. Unlike the steady state, the transient film exhibits often a change in concavity (curvature), depending on the flow parameters. The effects of draw ratio, inertia and gravity are summarized in the figure. The influence of D_R is depicted, for instance, upon

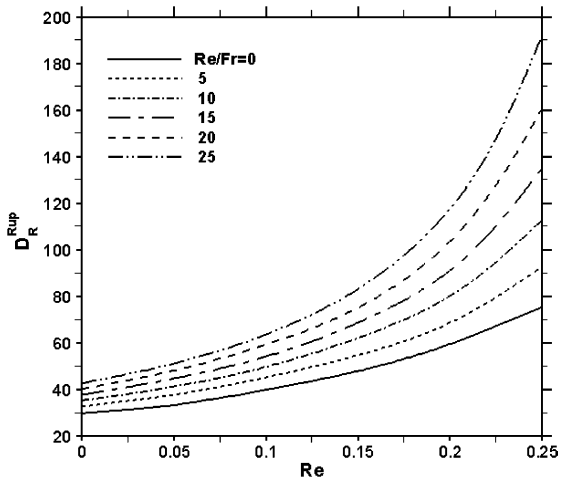

Fig. 13. Influence of inertia and gravity on the rupture draw ratio D_R^{Rup}, over the range $Re \in [0, 0.25]$, for different gravitational levels $Re/Fr \in [0, 25]$.

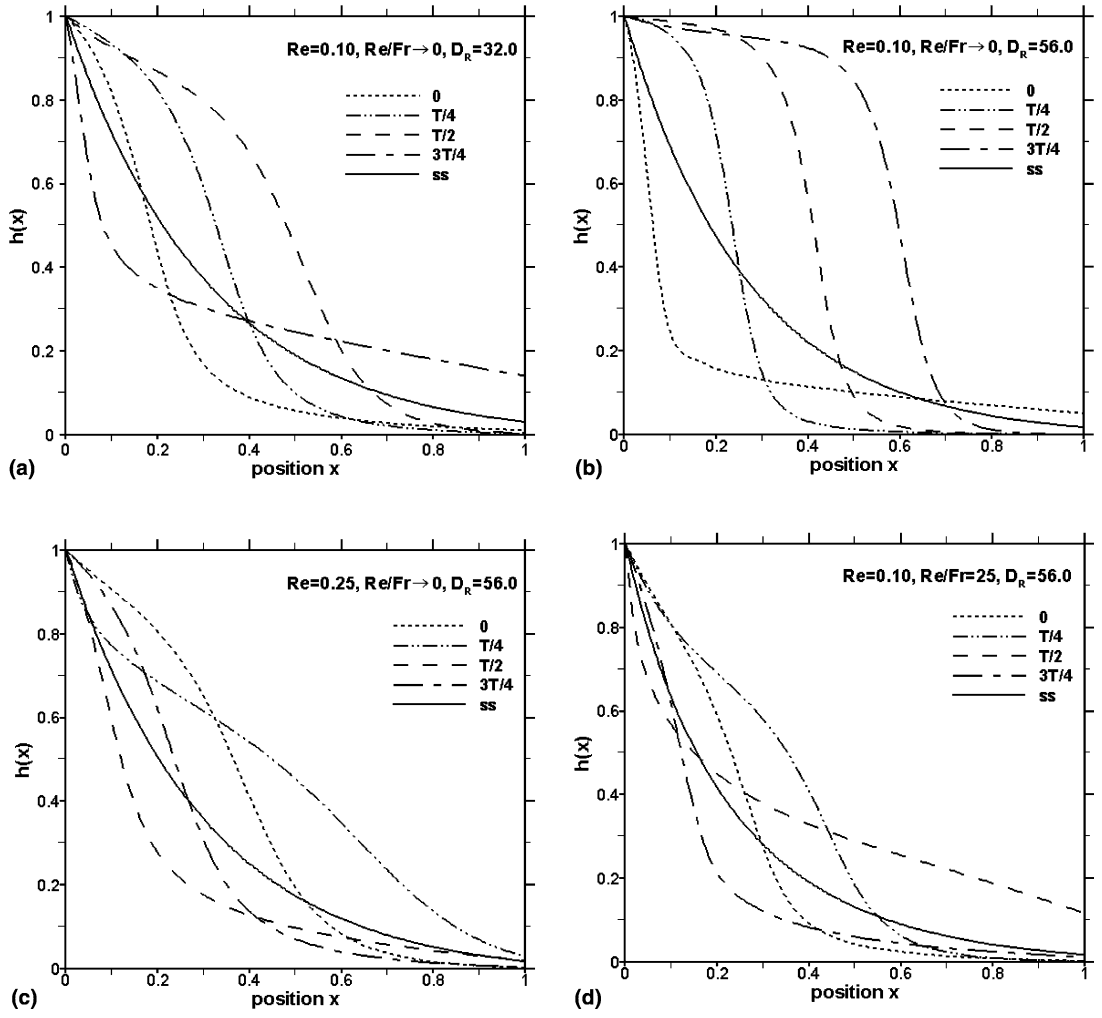

Fig. 14. Comparison of film shapes for various flow conditions during one oscillation period: (a) $D_R = 32.0$, $Re = 0.10$ (negligible gravity), (b) $D_R = 56.0$, $Re = 0.10$ (negligible gravity), (c) $D_R = 56.0$, $Re = 0.25$ (negligible gravity), (d) $D_R = 56.0$, $Re = 0.10$ and $Re/Fr = 25$. The corresponding steady-state film shapes are also shown.

comparison between Fig. 14(a) and (b), for $Re = 0.10$ and in the absence of gravity. In both cases, the film decreases sharply in thickness near the die exit at the beginning of the period ($t = 0$). The influence of inertia can be examined upon comparing Fig. 14(b) and (c), and that of gravity upon comparing Fig. 14(b) and (d). More generally, the film shape is close to the steady state for a flow near criticality (see Fig. 14(a), (c) and (d)). For a flow far from criticality, the film tends to remain relatively thick near $x = 0$ (h close to 1) for the remainder of the period, and decreases sharply downstream (see Fig. 14(b)). It is important to observe that at later times within a period of oscillation, the film thickness can remain relatively constant, equaling the very small thickness value at the take-up point, over a substantial portion of the air gap (see Fig. 14(b) again). In this case, the film does not necessarily rupture at the take-up point.

Finally, another important question emerges regarding the spatial response of the film under transient conditions, namely the dependence of the oscillatory behavior on position within the air gap. Fig. 15

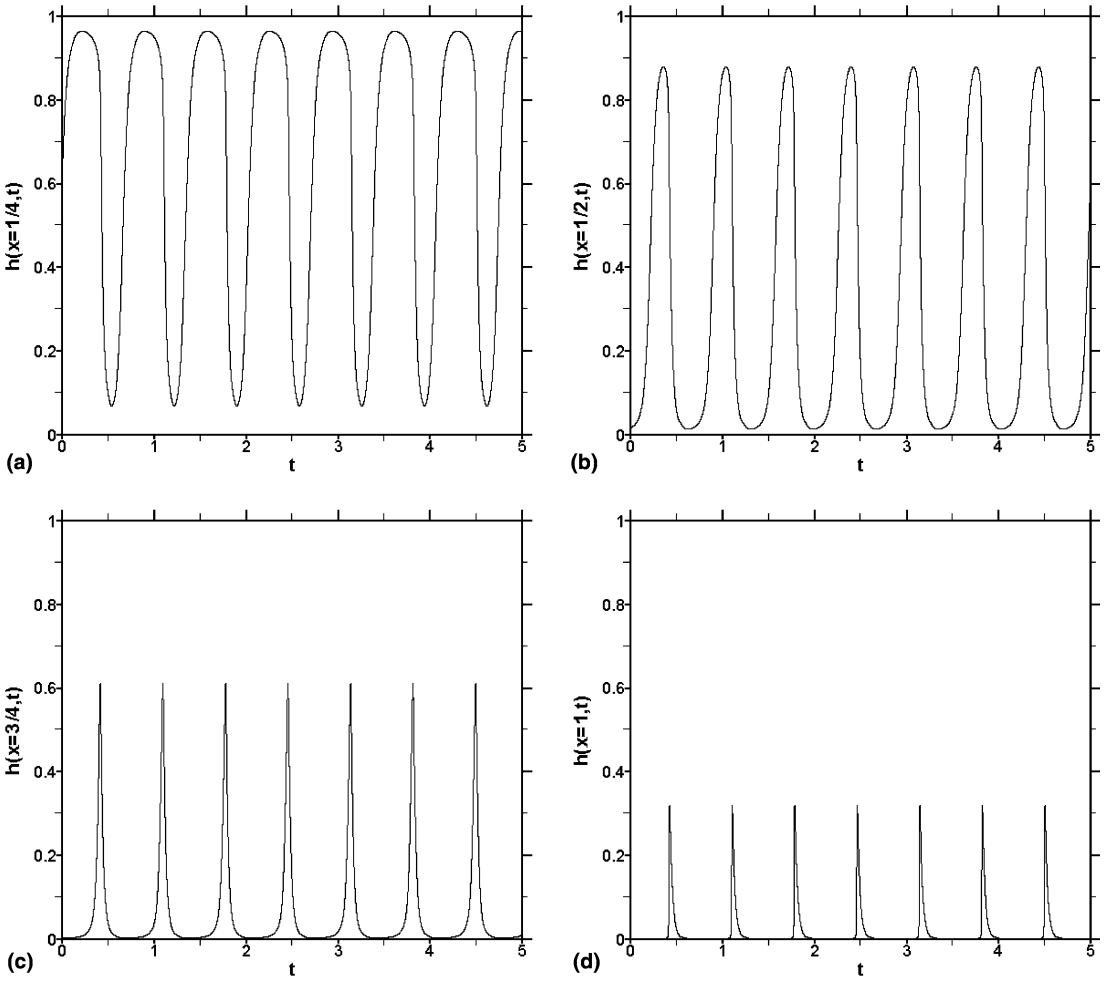

Fig. 15. Sustained oscillation $h(x,t)$ for $D_R = 56.0$ and $Re = 0.10$, in the absence of gravity, at different positions: (a) $x = 1/4$, (b) $x = 1/2$, (c) $x = 3/4$ and (d) $x = 1$.

illustrates the temporal thickness behavior for $D_R = 56.0$ and $Re = 0.10$ (gravity negligible) at different positions $x = 1/4$, 1/2, 3/4 and 1. It is shown that the film-thickness oscillation amplitude is much greater near the channel exit than close to the take-up point. It is interesting to observe that the whole system oscillates at the same frequency. This is somewhat surprising, especially for a flow far from criticality, where nonlinear effects are presumably strong; close to criticality, the whole film is of course expected to oscillate at the same frequency. The shape of waveforms in the figure indicates that near the die exit ($x = 1/4$), the oscillation exhibits broad arch peaks alternating with narrow bottoms. The film thickness varies over a large range of values. At the midpoint, the shape of the waveform is reversed, with the thickness approaching a smaller value over a longer time. This trend continues further downstream, with the peaks getting narrower and the bottoms getting wider, as typically illustrated in Fig. 15(c). At the take-up point (Fig. 15(d)), the amplitude is reduced by almost 70%, and the film thickness is essentially zero for most of the time, indicating that the film has practically ruptured.

5. Conclusions

The role of inertia and gravity in draw resonance is investigated for a Newtonian film. Both linear stability analysis, which predicts the critical threshold of instability, and nonlinear stability analysis, which focuses on the transient response, are carried out in this study.

For linear stability analysis, the eigenvalue problem is treated as a two-point boundary-value problem, including the steady state, which is determined simultaneously. Instead of being treated as a linear initial-value problem with shooting, the current method makes the eigenvalue problem nonlinear, avoiding the shooting scheme. The steady-state film thickness (velocity) is found to increase (decrease) with the increasing inertia. Gravitational effect has the opposite influence. Linear stability analysis indicates that both inertia and gravity have important effects on the onset of instability. It is found that while both inertia and gravity enhance the stability in film casting, inertia plays a dominant role and gravity helps stabilize the process rather mildly. Inertia has a significant influence on the stability picture even at small Reynolds number. Certain combinations of the flow parameters, lead to a dramatic increase in the critical draw ratio (e.g., for $Re = 0.25$ and $Fr = 0.10$, $D_R^C = 98.982$). The disturbance frequency also grows with increasing inertia and gravity, which implies that the system oscillates at a higher frequency when it loses stability. Results show that the frequency is more sensitive to the effect of gravity, contrary to the strong dependence of the critical draw ratio on inertia.

The critical draw ratio predicted by the linear stability analysis is verified by the nonlinear analysis for finite-amplitude disturbance. A finite-difference approach is applied to investigate the transient behavior of the film flow. At the critical draw ratio, the system oscillates harmonically, indicating the onset of a Hopf bifurcation. For a draw ratio above D_R^C, finite-amplitude disturbances are amplified and sustained oscillation is achieved. The oscillation thickness or velocity profile at the take-up point exhibits narrow, sharp peaks alternating with wide, flat bottoms. The decay or growth rate depends on the flow parameters.

The stabilizing effect of inertia and gravity from the linear stability analysis has also been confirmed through the nonlinear stability analysis. Results show that the nonlinearity can be effectively halted by inertia and gravity. It is predicted that the rupture of the film can also be delayed by inertia and gravity. In addition, the film oscillates less frequently but more fiercely for greater D_R. It is found that the film-thickness amplitude decreases with air-gap distance, but the film tends to rupture at the chill roll first.

Acknowledgment

This work was supported in part by Material and Manufacturing Ontario, and the Natural Science and Engineering Research Council of Canada.

References

Agassant, J.-F., Avenas, P., Sergent, J.-Ph., Carreau, P.J., 1991Polymer Processing: Principles and Modeling, vol. 23. Carl Hanser Verlag, New York, p. 226.

Aird, G.R., Yeow, Y.L., 1983. Stability of film casting of power-law liquids. Ind. Eng. Chem. Fund. 22, 7–10.

Alaie, S.M., Papanastasiou, T.C., 1991. Film casting of viscoelastic liquid. Polym. Eng. Sci. 31 (2), 67–75.

Anturkar, N.R., Co, A., 1988. Draw resonance in film casting of viscoelastic fluids: a linear stability analysis. J. Non-Newton Fluid. Mech. 28, 287–307.

Barq, P., Haudin, J.M., Agassant, J.F., Roth, H., Bourgin, P., 1990. Instability phenomena in film casting process. Int. Polym. Proc. V, 264–271.

Donnelly, G.J., Weinberger, C.B., 1975. Stability of isothermal fiber spinning of a Newtonian fluid. Ind. Eng. Chem. Fund. 14 (4), 334–337.

Doufas, A., McHugh, A., Miller, C., 2000. Simulation of melt spinning including flow-induced crystallization. Part I. Model development and predictions. J. Non-Newtonian Fluid. Mech. 92, 27–66.

Fisher, R.J., Denn, M.M., 1975. Finite-amplitude stability and draw resonance in isothermal melt spinning. Chem. Eng. Sci. 30, 1129–1134.

Gelder, D., 1969. The stability of fiber drawing processes. Ind. Eng. Chem. Fund. 10, 534–535.

Ishihara, H., Kase, S., 1975. Studies on melt spinning. V. Draw resonance as a limit circle. J. Appl. Polym. Sci. 19, 557–565.

Ishihara, H., Kase, S., 1976. Studies on melt spinning. VI. Simulation of draw resonance using Newtonian and power law viscosities. J. Appl. Polym. Sci. 20, 169–191.

Iyengar, V.R., Co, A., 1993. Film casting of a modified Giesekus fluid: a steady-state analysis. J. Non-Newtonian Fluid. Mech. 48, 1–20.

Iyengar, V.R., Co, A., 1996. Film casting of a modified Giesekus fluid: stability analysis. Chem. Eng. Sci. 51, 1417–1430.

Kumar, A., Gupta, R.K., 2003, 2nd ed.Fundamentals of Polymer Engineering Marcel Dekker, New York, p. 674.

Middleman, S., 1977. Fundamentals of Polymer Processing. McGraw-Hill, New York.

Pearson, J.R.A., Matovich, M.A., 1969. Spinning a molten threadline: stability. Ind. Eng. Chem. Fund 8 (4), 605–609.

Shah, Y.T., Pearson, J.R.A., 1972. On the stability of nonisothermal fiber spinning—general case. Ind. Eng. Chem. Fund. 11 (2), 150–153.

Yeow, Y.L., 1974. On the stability of extending films: a model for the film casting process. J. Fluid. Mech. 66, 613–622.